# Ultrasonic Impact Treatment: Assessing the Process Energetics

S. P. Chenakin, B. M. Mordyuk, N. I. Khripta, and V. Yu. Malinin

*G. V. Kurdyumov Institute for Metal Physics, N.A.S. of Ukraine,*
*36 Academician Vernadsky Blvd.,*
*UA-03142 Kyiv, Ukraine*

A comparative study of process energetics is carried out for two loading schemes being used in ultrasonic impact treatment of materials, namely, a single-pin normal impacting mode and a multipin sliding/shearing impacting mode involving a low-frequency reciprocating motion of the sample. The maximum kinetic energy (or velocity) and frequency of stochastic oscillations of pins are measured experimentally for both loading modes at ultrasonic horn amplitudes varying in the range from 16 μm to 28 μm. Accordingly, a number of impact parameters such as impact time, maximum impact force, maximum impact stress, energy density and power density injected per impact in the contact area, total energy and power densities deposited in the sample (ZrTiNb alloy in this case) during treatment time are assessed. Variation of these impact characteristics is considered for both modes as a function of the ultrasonic horn amplitude, number of pins in the impact head (in sliding mode), pins' dimensions and material of the sample. The effect of amplitude and frequency of reciprocating sample holder in sliding impact mode on the total energy density deposited across the sample surface is analysed. The evaluated parameters are expected to be helpful in understanding the impact treatment-induced changes in physicochemical characteristics of various materials.

**Key words:** ultrasonic impact treatment, pin velocity, pin impact frequency, impact parameters, ZrTiNb alloy

Проведено порівняльне дослідження енергетики процесу для двох схем навантаження, які використовуються в ультразвуковому ударному обробленні матеріялів, а саме, для: нормального ударного режиму з одним бияком і режиму ковзного/зсувного удару кількома бияками із низькочас-

Corresponding author: Sergiy Petrovych Chenakin
E-mail: chenakin@imp.kiev.ua

тотним зворотньо-поступальним рухом зразка. Експериментально вимі-
ряно максимальну кінетичну енергію (або швидкість) і частоту стохасти-
чних коливань бияків для обох режимів навантаження за амплітуд коли-
вання ультразвукового концентратора в діяпазоні від 16 мкм до 28 мкм.
Відповідно, проведено оцінку ряду параметрів удару, таких як час удару,
максимальна сила удару, максимальне ударне напруження, густина ене-
ргії та густина потужности, що акумулюються під час удару у зоні конта-
кту, та загальні густини енергії й потужности, що передаються зразку
(стопу ZrTiNb в даному випадку) за час ударного оброблення. Розглянуто
варіяції цих ударних характеристик для обох режимів оброблення в зале-
жності від амплітуди ультразвукового концентратора, кількости бияків в
ударній голівці (у режимі ковзного удару), розмірів бияків і матеріялу зра-
зка. Проаналізовано вплив амплітуди та частоти зворотньо-поступального
руху утримувача зразка в режимі ковзного удару на загальну густину ене-
ргії, що акумулюється на поверхні зразка. Очікується, що оцінені парамет-
ри уможливлять зрозуміти зміни фізико-хемічних характеристик різних
матеріялів, спричинені ударним обробленням.

**Ключові слова:** ультразвукове ударне оброблення, швидкість бияка, час-
тота ударів бияка, енергетичні параметри удару, стоп ZrTiNb.

## 1. INTRODUCTION

To date, a number of various techniques for modifying the surface of
materials have been proposed, in particular, methods that provide sur-
face severe plastic deformation (SSPD). These methods inducing grain
refinement, generating compressive residual stresses, affecting the
surface roughness and modifying the surface chemical state are being
leveraged to produce materials with superior surface integrity and ex-
cellent properties, which have found their application in different
fields. In order to opt for an appropriate method to be employed for
surface modification, it is necessary to understand the similarities and
differences as well as the limitations and advantages of the processes
underlying the SSPD methods by comparing the effect of treatment
parameters on the materials' structure and properties.

A comparative study [1] of effects of conventional shot peening (SP)
and surface mechanical attrition treatment (SMAT) of a 316L stainless
steel performed with the same Almen intensity and the same coverage
revealed that SP resulted in a higher fatigue life under low strain am-
plitude, but lower fatigue life under high strain amplitude as com-
pared to the SMATed samples. A numerical simulation of the SP and
SMAT processes [2] shows that under the same impact kinetic energy,
the SP-induced plastic strain rate is larger than that of SMAT and, for
the same coverage, the grain refinement caused by severe SP (SSP) is,
accordingly, stronger than that by SMAT, whereas SMAT induces

larger compressive residual stresses and much smaller surface roughness than SP. SMAT with multiple shot incidence angles and shot oblique impacts is found to be more efficient for surface compressive residual stresses and grain refinement as compared to SP with shot incidence angle of 90°. When compared to laser shock peening (LSP), SP of a 316L steel was observed [3] to bring about larger work hardening, surface roughening and residual compressive stress levels because of a more severe surface loading; at the same time, LSPed sample exhibited a better pitting corrosion resistance. Ultrasonic impact peening (UIP) of a 316L stainless steel with a peening needle having a semi-ellipsoid tip [4] and UIP of an AISI 321 stainless steel with a disk-shaped flat pin [5] was shown to also produce a much higher level of the compressive residual stress, appreciably stronger work hardening and much smaller grain size than LSP.

Gill *et al.* [6] employed LSP, cavitation peening (CP) in air and water and ultrasonic nanocrystal surface modification (UNSM) with a WC ball tip under different loads to improve properties of Inconel 718 superalloy. UNSM was found to provide the highest increase in hardness and the highest level of residual compressive stress due to higher plastic deformation as compared to CP and LSP. The observed differences in roughness, hardness, residual stresses and microstructure induced by all three peening techniques were shown to be dependent on the way the plastic deformation takes place. Maleki *et al.* [7] also found UNSM to be the most efficient method in improving the mechanical properties of Inconel 718 in comparison with SSP and LSP, giving rise to the strongest increase in the surface hardness, largest average depth of the affected layer, highest level of residual compressive stress, longest fatigue life and strongest grain refinement followed by SSP and LSP. By comparing the effects of LSP, water jet cavitation peening (WjCP), water jet shot peening (WjSP), and multipin ultrasonic impact treatment (UIT) on AISI 304 stainless steel, Lesyk *et al.* [8] determined the optimal treatment regime for each technique that provided maximum surface hardness and compressive residual stress along with minimum surface roughness. The strongest work hardening and maximum reduction in roughness parameter attained by each method were obtained to decrease in the sequence UIT > WjSP > WjCP > LSP. Soyama demonstrated [9] that treatment of a 316L stainless steel by using water jet peening (WjP), CP, SP, and LSP with an optimum coverage improved the fatigue performance of the steel, with the highest fatigue strength/fatigue life being obtained with CP/SP followed by SP/CP, LSP and WjP and closely related to Vickers hardness/residual stress and the surface roughness. The effects of SP, SMAT, LSP, UNSM and surface mechanical rolling treatment (SMRT) on the fatigue properties of metals and their dependence on the surface finish, microhardness, residual stress and microstructure of the treated materials were reviewed

and compared by Rui Chen *et al.* [10]. To understand comprehensively the effects caused by the various peening methods and compare quantitatively their effectiveness, impact velocities/energies and strain rates were assessed for SMAT [11], SP and SMAT [2], SP, CP and LSP [12].

As distinct from other ultrasonically assisted peening techniques such as UIP (using a needle-shaped striker connected to an ultrasonic horn) [4], UNSM (using WC, $Al_2O_3$ or $Si_3N_4$ ball tip pressed by a horn) [6, 7] or SMAT (using a large number of steel balls as strikers) [2, 11], UIT devices convert ultrasonic energy into multiple stochastic impacts of an intermediate element (pin or pins) freely oscillating with a high velocity in the gap between the ultrasonic horn tip and the treated surface. In our laboratory, two different loading schemes are being used for UIT of materials, namely, single-pin normal impact mode and sliding/shearing multipin mode [13]. The energy of pins in the UIT process is a key parameter determining the strain rate, which plays a crucial role in the plastic strain-induced phenomena occurring both on the surface (*e.g.*, oxidation [14], nitriding [15], hardening [14, 16], *etc.*) and in the subsurface layers (residual stress accumulation and grain refinement [13, 16]). However, in previous UIT-related papers only tentative values of energy parameters based on some general conceptions were used. In a recent work [17], we performed a comparative study of the impact energy effects of the two UIT loading schemes on the structural state, surface chemical and phase composition, roughness, microhardness, and corrosion properties of a Zr−31Ti−18Nb alloy. In the present work, we explore the energetics of both UIT loading modes and evaluate a number of energy parameters as a function of experimental conditions that can affect the treatment process and can be useful for understanding the differences in the UIT-induced alterations.

## 2. EXPERIMENTAL

The instrument for UIT comprises a piezoceramic transducer with an ultrasonic horn. The ultrasonic horn driven by a 1 kW ultrasonic generator and vibrating with a frequency of 21 kHz transfers its kinetic energy to the sample via repetitive impacts by the pin/pins positioned between the horn flat tip and the sample surface. Before processing, the ultrasonic system is typically pressed against the sample at a static load of 50−90 N. In this case, the total energy applied to the material is the sum of the static energy imposed by the pressed ultrasonic device and the dynamic energy resulting from the ultrasonic vibration [6].

In one loading scheme, a single disk-shaped pin obtaining its energy from the ultrasonic horn produces repetitive normal impacts on the unconstrained sample placed in the holder on a supporting disk, so that the sample experiences mainly compressive (axial) deformation, with the radial expansion being small (Fig. 1, *N*). We call this scheme the
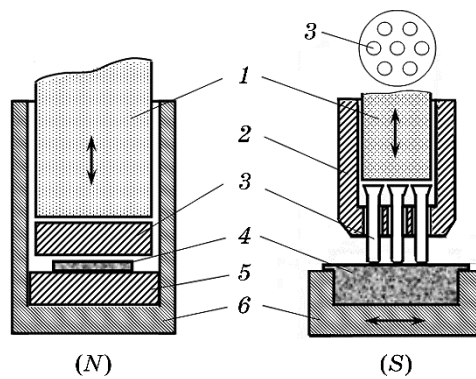
**Fig. 1**. Ultrasonic impact treatment schemes: single-pin normal impact loading mode (*N*) and sliding/shearing multi-pin impact loading mode (*S*): *1*—vibrating ultrasonic horn, *2*—impact head, *3*—pins, *4*—sample, *5*—bearing steel disk support, *6*—sample holder.

single-pin normal impact-loading mode (denoted for brevity *N*). This mode was used, *e.g.*, for UIT of AISI 321 stainless steel [5, 18] and Zr–Ti–Nb alloy [19]. In a modified version of this loading scheme [14, 15, 20], the (constrained) sample is fitted into a cylindrical pit in the sample holder and experiences only axial deformation.

In the other loading scheme [8, 13, 16, 21], a special impact head with seven rod-like pins is mounted on the horn tip (Fig. 1, *S*). When the ultrasonic vibrations are switched on, the pins start to oscillate stochastically in the gap formed between the horn tip and sample surface. Besides, during UIT in this mode, the sample holder reciprocates with a frequency $f_s$ and amplitude $A_s$, which can be independently adjusted. Under such conditions, the pins would produce repetitive sliding impacts on the sample surface. Accordingly, we call this processing scheme the sliding/shearing multipin impact-loading mode (for brevity, referred to as mode *S*).

To assess the energetics of the impact treatment process, we need to know the kinetic energy/velocity of the pin/pins and the frequency of its/their oscillations. The vibration frequency $f_{uh}$ and amplitude $A_{uh}$ of ultrasonic horn tip are the main parameters that determine the maximum vibration velocity ($V_{uh} = 2\pi f_{uh} A_{uh}$) and acoustic pressure, which is created nearby the horn tip and is considered the main driving force to propel pins to a maximum velocity.

For measuring kinetic energy acquired by the pin, we used an approach similar to that employed for evaluation of the maximum impact velocities of balls during SMAT [11] and SP [12] processes. Accordingly, we mounted an experimental set-up with an acoustic system that was positioned vertically, and the pins which are being used in modes *N* and *S* were placed on the top of the horn tip (Fig. 2, *a*). Upon switching

on the ultrasonic vibration, the pin leapt up to a certain attitude. These leaps were filmed by a high-speed camera (Nickon Coolpix 4500) to capture the upward motion of the pins. By choosing an appropriate frame, we could measure the maximum height $h$ reached by the pin. As an example, Fig. 2 shows the frames fixing the highest attitude attained by one (Fig. 2, $b$) and three rod-like pins (Fig. 2, $c$) being used for UIT in sliding ($S$) mode and by a disk-shaped pin (Fig. 2, $d$) being used in normal ($N$) mode. Since the maximum height of the pin rise depended on the ultrasonic horn amplitude setting, prior to the experiments, the actual amplitude of the ultrasonic horn tip was measured by using a non-contact piezoceramic vibrometre AVM-4M. The maximum kinetic energy acquired by the pin from the vibrating horn tip at different $A_{uh}$ was determined from its equality to the potential energy of the pin at the highest attitude $E = mgh$, where $m$ is the mass of the pin, $g$ the acceleration of gravity.

In order to evaluate the frequency of impacts of oscillating pins, we performed additional experiments in which the gaps between the sample surface and vibrating ultrasonic horn produced by oscillating pins were measured for different $A_{uh}$. As an example, Figs. 2, $e$ and $f$ show frames of the loading unit with marked gaps formed during UIT processing of the sample in modes $S$ and $N$, respectively. Actually, the gap size should correspond to the maximum path of the pin striking the sample surface. However, the pin might fly a shorter distance than the established gap since the pins' path would depend on occasional collisions between the vibrating horn tip and the rebounding pin (horn tip may either accelerate or decelerate the pin). Despite the random char-
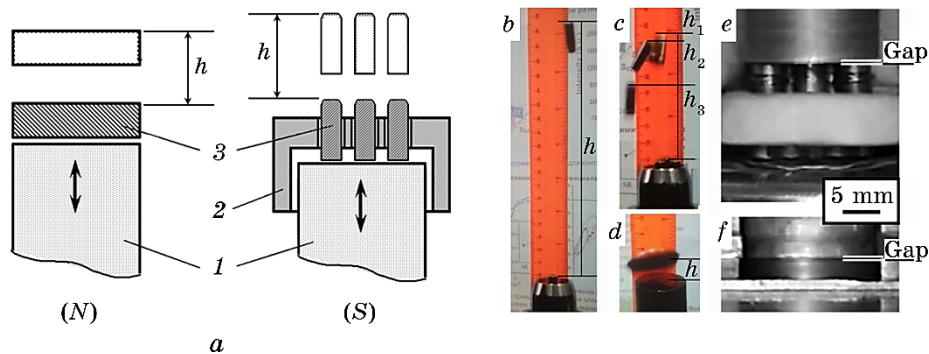


**Fig. 2.** Schematics ($a$) of the experimental setup for measuring the kinetic energy of pins in modes $N$ and $S$. The frames taken by a high-speed camera show the maximum height $h$ of rise of the pins upon switching on the vibrations of the horn tip in modes $S$ ($b$—one-pin set, $c$—three-pin set) and $N$ ($d$). The gaps formed by oscillating pins between the sample surface and vibrating ultrasonic horn are shown in frames for modes $S$ ($e$) and $N$ ($f$).

acter of the energy obtained by the pin from the horn and regardless of the pins' rebound distance, the energy transfer efficiency at any moment of the horn–pin collision and, accordingly, the magnitude of the acquired kinetic energy of the pin are expected to be always high due to the high vibration frequency of the horn tip (21 kHz). In a stationary process, the frequency $f_p$ of stochastic oscillations of the pin can be estimated from the size $A_g$ of the formed gap and the maximum velocity $V_p$ of the pin as $f_p = V_p / 2\pi (A_g / 2)$.

A foil of a Zr–31Ti–18Nb alloy 4 mm thick served as a sample for a comparative study of the effect of impact treatment energy deposited in two loading modes $N$ and $S$. In the present experiments, a disk-shaped pin used for UIT in mode $N$ had a mass of 6.04 g and was 17.5 mm in diameter and 2.8 mm thick. All rod-like pins used for impact processing in mode $S$ had a mass of 2.2 g and were 4.9 mm in diameter and 14.9 mm long. All the pins were made of hardened bearing steel ШХ-15 (analogue of AISI52100) with the composition in wt.%: 1.5 Cr, 1 C, 0.5 Cu + Ni, 0.3 Mn, 0.25 Si, < 0.02 S, balance Fe, $HB \cong 195$.

## 3. RESULTS AND DISCUSSION

As can be seen in Fig. 3, $a$, with increasing amplitude of the ultrasonic horn from 16 to 28 μm, the maximum kinetic energy $E_p$ of the disk-shaped pin measured as described above (see Fig. 2, $a$, $d$) strongly increases from $0.89 \pm 0.14$ mJ to $3.55 \pm 0.22$ mJ (curve $1N$). Accordingly, the derived maximum velocity of the pin $V_p$ changes from 0.54 to 1.08 m/s. The maximum kinetic energy of a rod-like pin measured in a set of one, three (see Fig. 2, $a$–$c$), five and seven pins increases with increasing $A_{uh}$ more slowly than $E_p$ ($1N$) and decreases with increasing the number of pins in the impact head (Fig. 3, $a$, curves $1S$–$7S$). In particular, $E_p$ of the pin in the one-pin set increases with amplitude from $2.27 \pm 0.09$ to $3.09 \pm 0.12$ mJ (curve $1S$), and $E_p$ imparted to one pin in a seven-pin set changes from $0.26 \pm 0.07$ to $0.36 \pm 0.08$ mJ ($V_p$ changes from 0.49 to 0.57 m/s) (curve $7S$). Note that in the range of $A_{uh}$ from 16 to 23 μm the kinetic energy of one pin (or total $E_p$ of all pins) being used in mode $S$ is higher than $E_p$ of the pin being used in mode $N$, whereas at an amplitude of 28 μm $E_p$ of the pin in mode $N$ exceeds that in mode $S$ (Fig. 3, $a$).

The variation of the size of the gap $A_g$ between the sample surface and vibrating ultrasonic horn measured for the set of three, five and seven pins in mode $S$ and for one pin in mode $N$ is presented in Fig. 3, $b$ as a function of the horn amplitude. It shows that, at $A_{uh}$ greater than $\cong 10$ μm, the gap produced in mode $N$ becomes larger than that in mode $S$. The most probable frequency $f_p$ of impacts of oscillating pins in modes $N$ and $S$ derived from the gap size $A_g$ and the maximum pin velocity $V_p$ is shown in Fig. 3, $c$ as a function of $A_{uh}$. It can be seen that in
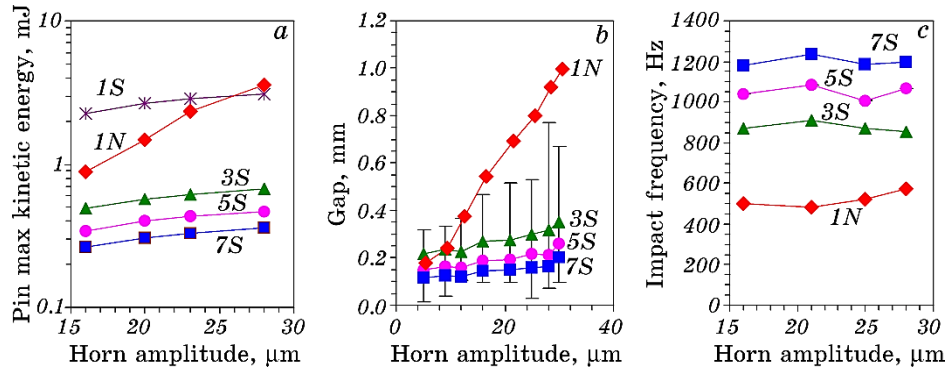
**Fig. 3.** Variation of maximum kinetic energy of pins (*a*), size of the gap formed between the ultrasonic horn tip and the sample (*b*) and frequency of impacts of oscillating pins (*c*) being used for processing in the normal impact mode (*N*) and sliding impact mode (*S*) as a function of amplitude of the ultrasonic horn. The labelling of the curves indicates the number of pins and the processing mode.

the range of amplitudes from **16** to **28** µm, the average $f_p$ is practically independent of $A_{uh}$ and is estimated to be $520 \pm 64$ Hz for the pin in mode $N$ and $875 \pm 192$ Hz, $1050 \pm 233$ Hz, and $1200 \pm 267$ Hz for three, five and seven pins, respectively, in mode $S$. The obtained frequencies of impacts suggest that the mechanical processing with the given UIT devices can actually be specified as ultrasonically driven high-frequency mechanical impact (HFMI) treatment.

By making use of the experimentally determined values of $E_p$, $V_p$ and $f_p$, we evaluated a number of energy parameters that can affect the treatment process and can be suitable for comparison of the UIT-induced alterations under both loading schemes.

Let us define the quantity $E_r$ [J·s$^{-1}$] $= E_p f_p$ as the energy deposition rate. Then the total maximum mechanical energy transferred to the sample during UIT for time $t$ amounts to $E_m$ [J] $= E_r t = E_p f_p t$.

Under the same impact kinetic energy $E_p$, the intensity of impact load and, accordingly, its effect will depend on the contact area between the pin and the target surface [2]. The expression $E_0$ [J/cm$^2$] $= = E_p/S$, where $S$ is the impact spot area, represents the specific peak energy density deposited in an impact. Then, $E_i$ [J·s$^{-1}$·cm$^{-2}$] $= E_0 f_p = = E_r/S = E_p f_p/S$ will describe the impact energy intensity in the contact area or the specific energy deposition rate in the impact spot area, with the total energy deposited in the impact area during UIT being $E_t$ [J/cm$^2$] $= E_i t = E_0 f_p t$.

The peak power density injected per impact in the contact area can be defined as $P_0$ [W/cm$^2$] $= E_p/(\tau S)$, where $\tau$ is the duration of a single impact. Then, the total mechanical power applied to the contact area of

the material during UIT is described as $P_t\,[\mathrm{W/cm^2}] = P_0 f_p t$.

The impact time can be derived from Newton's second law as $\tau = m_p \Delta V_p / F$, where $m_p$ is the mass of a pin, $\Delta V_p$ the change of the pin velocity during impact (from max to 0), $F$ the maximum impact force of a pin. The latter can be evaluated according to an energy model of impact [22] as $F = V_p (m_p k_s / (1 + k_s / k_p))^{1/2}$; here, $k_s = E(s)S_s / l_s$ and $k_p = E(p)S_p / l_p$ stand for the stiffness of the sample and the pin, respectively, with $E(s)$, $E(p)$ being the elastic moduli (59 GPa for the Zr31Ti18Nb sample and 211 GPa for the ШХ-15 bearing steel pins), $S_s$, $S_p$ the cross-sectional areas and $l_s$, $l_p$ the lengths of the sample and the pin. For a given set of pins and a sample, the maximum impact force in the normal impact mode in the range of $A_{uh}$ from 16 to 28 µm was estimated to grow from $1468 \pm 581$ to $2936 \pm 949$ N. This is significantly larger than $F$ in the sliding impact mode, which decreases with increasing number of pins and changes, *e.g.*, from $466 \pm 53$ to $544 \pm 62$ N, when using 3 pins, and from $341 \pm 39$ to $398 \pm 45$ N for 7 pins. Accordingly, the impact time $\tau$ was evaluated to be $2.13 \pm 1.05$ µs in mode $N$ and $3.83 \pm 1.31$ µs in mode $S$ (for any number of pins).

As can be seen in Fig. 4, *a*, the evaluated energy deposition rate $E_r$ increases with increasing $A_{uh}$ and with increasing number of pins in mode $S$, in this mode, $E_r$ is significantly larger than that in mode $N$. The impact energy density $E_0$ deposited in the contact area also increases with increasing horn amplitude but, on the contrary, decreases with increasing number of pins in mode $S$, in mode $N$, $E_0$ is higher than that in 7-pin mode $S$ in the entire range of $A_{uh}$ (Fig. 4, *b*). Like $E_0$, the
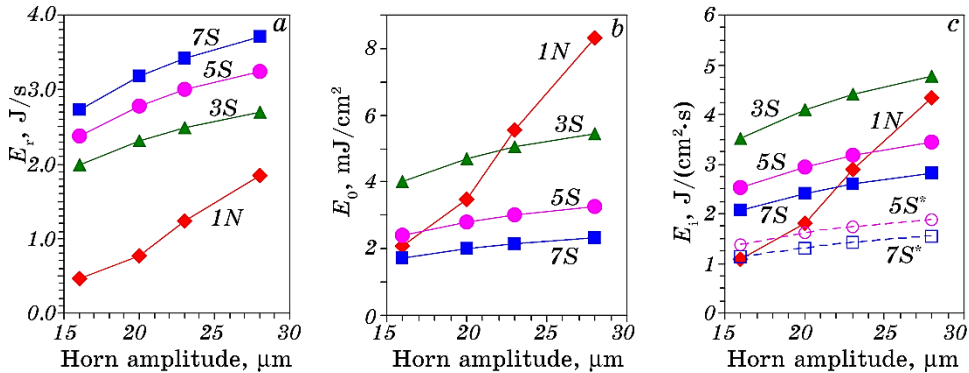


**Fig. 4.** Variation of energy deposition rate $E_r$ (*a*), peak energy density deposited in an impact spot area $E_0$ (*b*) and impact energy intensity in the contact area $E_i$ (*c*) during processing in the normal impact mode ($N$) and sliding impact mode ($S$) as a function of amplitude of the oscillating ultrasonic horn. The labelling of the curves indicates the number of pins and the processing mode. The dashed-line curves $5S^*$ and $7S^*$ shown in (*c*) represent the impact intensity $E_i$ corrected for reciprocating motion of the sample in 5- and 7-pin mode $S$.

impact load intensity in the contact area $E_i$ increases with $A_{uh}$ and decreases with number of pins but in mode $N$; $E_i$ appears to be larger that this is in 7-pin mode $S$ only at amplitudes above 23 µm (Fig. 4, $c$).

The specific power density $P_0$ injected per impact in the contact area rises with $A_{uh}$ and decreases with increasing number of pins in mode $S$, at amplitudes above 16 µm, $P_0$ in mode $N$ appreciably exceeds that in mode $S$ for 3, 5 and 7 pins (Fig. 5, $a$). Specifically, $P_0$ rises from 0.98 to 3.91 kW/cm$^2$ in mode $N$ and from 0.45 to 0.61 kW/cm$^2$ in 7-pin mode $S$. As compared to $P_0$, the total power density $P_t$ evaluated for the impact treatment time $t = 2$ min (which was found [14, 15, 17, 19] to be optimal in UIT of different materials) demonstrates enhanced values in mode $S$ (due to a higher $f_p$) so that $P_t$ in mode $N$ becomes larger than that in 3-, 5- and 7-pin mode $S$ only at $A_{uh} > 23$ µm (Fig. 5, $b$). Specifically, in mode $N$, $P_t$ rises with $A_{uh}$ from 61.0 to 244.2 MW/cm$^2$ and in 7-pin mode $S$ from 64.7 to 88.1 MW/cm$^2$. Note that the total mechanical energy $E_m$ transferred to the sample and the total energy density $E_t$ deposited in the impact area evaluated for $t = 2$ min change with $A_{uh}$ qualitatively in the same way as $E_r$ and $E_i$, respectively (cf. Fig. 4, $a$ and $c$), differing from $E_r$ and $E_i$ by a factor of $t$.

The maximum impact stress arising in the sample section, $\sigma_{max} = F/S$, can be estimated [22] as $\sigma_{max} = V_p\{3\rho_s E(s)\}^{1/2}$, where $\rho_s$ is the sample density (6346 kg/m$^3$ for Zr31Ti18Nb alloy). It can be seen in Fig. 5, $c$ that $\sigma_{max}$ increases with increasing $A_{uh}$, and decreases with increasing number of pins in mode $S$, at $A_{uh} > 16$ µm, $\sigma_{max}$ in mode $N$ exceeds that in 7-pin mode $S$.

In evaluating the energy characteristics such as $P_t$ and $E_t$ integrated
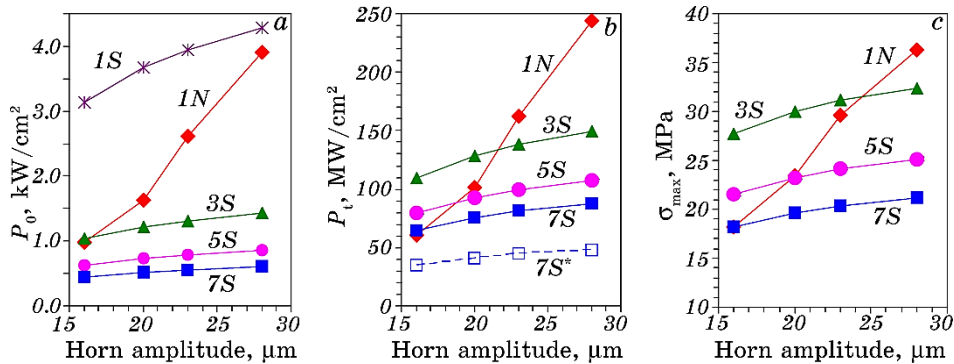


**Fig. 5.** Variation of impact power density $P_0$ injected in the contact area ($a$), total power density $P_t$ deposited during UIT for 2 min ($b$) and maximum impact stress $\sigma_{max}$ in the sample section ($c$) produced in the normal impact mode ($N$) and sliding impact mode ($S$) as a function of amplitude of the ultrasonic horn. The labelling of the curves indicates the number of pins and the processing mode. The dashed-line curve $7S^*$ shown in ($b$) represents $P_t$ corrected for reciprocating motion of the sample in 7-pin mode $S$.

over the treatment time $t$, reciprocating motion of the sample holder during UIT in mode $S$ has to be taken into account. Figure 6 shows an ideal model representation of imprints produced by impacts of oscillating pin ($f_p = 1200$ Hz) across the sample during a half-period of its reciprocating displacement with $f_s = 20$ Hz and amplitude $A_s$ of 8 mm (*a*) and 12 mm (*b*). One can see that within the sample boundaries, the number $Y_n$ of overlapped areas $S_n$ of the pin imprints with a particular number $n$ of impacts in the area as well as the number of impacts $n$ in a particular overlapped area decrease with increasing $A_s$ (*e.g.*, $Y_n = 22.5$, $n_{max} = 9$ for $A_s = 8$ mm and $Y_n = 15$, $n_{max} = 6$ for $A_s = 12$ mm).

Sample reciprocation results in a decrease in the density of deposited energy and its non-uniform distribution, with the $E_t$ and $P_t$ decreasing from the central part to the periphery (*cf.* Fig. 6). Besides, due to sample displacement, the just-impacted area would not be hit again in $1/f_p$ seconds and would have more time for relaxation. To correct the energy parameters for reciprocating motion of the sample, we evaluated the total energy densities $E_t^*$ and $P_t^*$ deposited across the sample surface by taking into account the number $Y_n$ of overlapped areas $S_n$ of the pin imprints and the number $n$ of impacts in these overlapped areas as:

$$E_t^* = 2f_s t \sum_{n=1}^{n_{max}} \frac{S_n}{S_p} n E_0 Y_n = 2E_0 Y_{n_{max}} f_s t, \quad P_t^* = 2f_s t \sum_{n=1}^{n_{max}} \frac{S_n}{S_p} n P_0 Y_n = 2P_0 Y_{n_{max}} f_s t.$$

The dashed line curves $5S^*$ and $7S^*$ in Fig. 4, *c* and curve $7S^*$ in Fig.
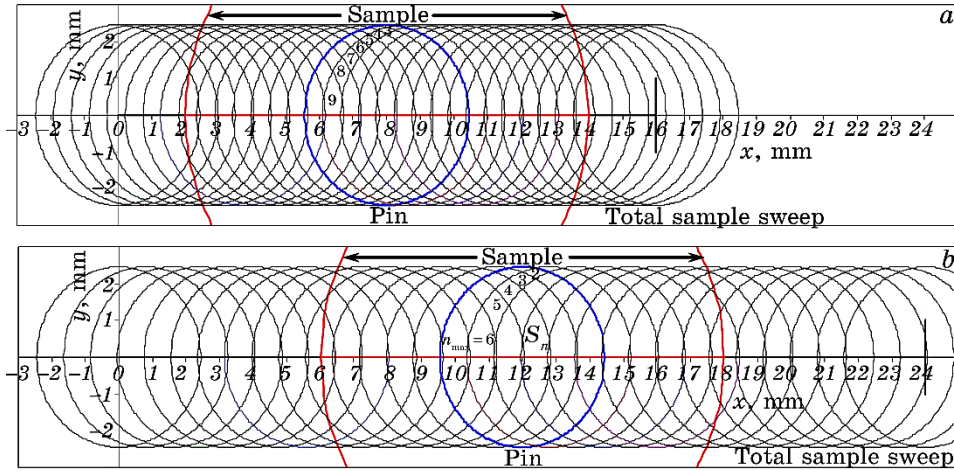


**Fig. 6.** Ideal representation of imprints produced in mode $S$ by the pin impacts on the sample during a half-period of its reciprocating displacement with $f_s = 20$ Hz and amplitude $A_s$ of 8 mm (*a*) and 12 mm (*b*) for $f_p = 1200$ Hz. Numerical characters (in italic) indicate the number $n$ of impacts in particular overlapped areas $S_n$.
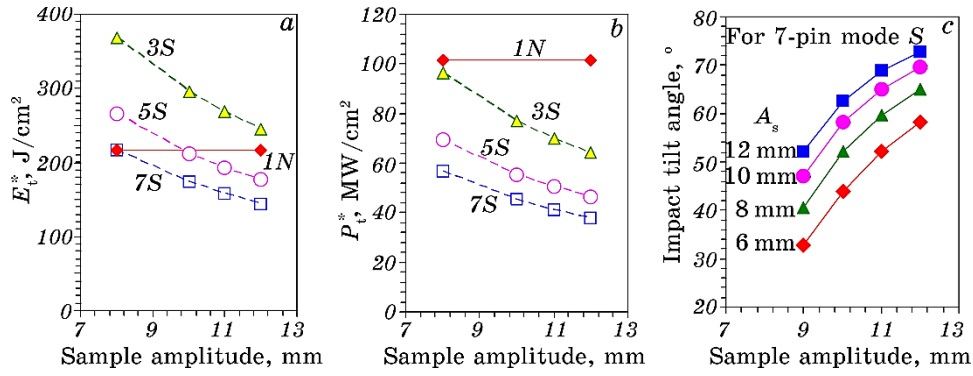
**Fig. 7.** Variation of corrected total energy density $E_t^*$ (*a*) and corrected total power density $P_t^*$ (*b*) deposited during UIT for 2 min as a function of the sample shift amplitude $A_s$ at $A_{uh} = 20$ µm. The labelling of the curves indicates the number of pins and the processing mode. Variation of the pin impact tilt angle (*c*) as a function of the sample shift frequency $f_s$ for different sample shift amplitudes $A_s$ in 7-pin mode at $A_{uh} = 20$ µm.

5, *b* represent the variation of respectively impact energy density $E_i^*$ and total power density $P_t^*$ corrected for reciprocating motion of the sample in 5- and 7-pin mode with $f_s = 20$ Hz and $A_s = 11$ mm as a function of horn amplitude. Note that the sample shift frequency $f_s$ do not affect the impact energy parameters, whereas the sample shift amplitude $A_s$ does. As can be seen in Fig. 7, the total energy density $E_t^*$ (*a*) and the total power density $P_t^*$ (*b*) deposited across the sample during $t = 2$ min decrease with increasing $A_s$.

Note also that a pin impinging normally on a reciprocating sample would experience a tilt by an angle determined by the ratio between the normal (pin) and lateral (sample) velocity components. Accordingly, the impact tilt angle β (with respect to the surface normal) will decrease with increasing $A_{uh}$ (or pin kinetic energy) and increase with increasing number of pins. Specifically, with increasing $A_{uh}$ from 16 to 28 µm the evaluated tilt angle of the pin in a 7-pin set striking the sample reciprocating with $f_s = 10$ Hz and $A_s = 10$ mm changes from 49 to 45°, at $A_{uh} = 20$ µm, β amounts to 35, 42 and 47° for 3-, 5- and 7-pin set, respectively. Besides, β will increase with increasing the sample shift frequency $f_s$ and amplitude $A_s$ (Fig. 7, *c*). One can speculate that tilting of the pin would decrease the impact contact area and thus increase the deposited energy and power densities $E_t^*$, $P_t^*$. On the other hand, the decrease in the contact area would decrease overlapping of the pin imprints, thus reducing $E_t^*$ and $P_t^*$ so that the possible effect of pin tilting on the actual energy density deposition cannot be definitely specified.

The impact energy parameters can be adjusted by changing not only the amplitude of ultrasonic horn and the treatment time but also the

pin dimensions (diameter, length, mass, material), which define the pin energy/velocity as well. The data presented in Table 1 show that the magnitudes of $P_0$ and $\sigma_{max}$ evaluated, as an example, for two types of pins being typically used in UIT are smaller and impact time $\tau$ is longer for larger (heavier) pins impacting the same ZrTiNb sample in both modes at the same $A_{uh} = 20$ µm. One can also see that the impact parameters evaluated for different samples (ZrTiNb, TiAlV, steel) of the same size are also dependent on the target material.

Ultrasonic impact treatment of a CrCoNi coating performed for 2 min with different amplitudes (0, 10, 15 and 20 µm) has shown [23] that depth of the impacted layer, microhardness, refinement of the top grains and wear resistance of the coating increase with increasing horn amplitude that can be related with a corresponding augmentation of different energy parameters evaluated in our study (*cf.* Figs. 4, 5). A greater extent of deformation-induced oxidation, stronger structural alterations, higher microhardness and corrosion resistance observed for ZrTiNb alloy after UIT for 2 min at $A_{uh} = 20$ µm in mode $N$ as compared to 7-pin mode $S$ were shown [17] to also correlate well with parameters $E_0$, $P_0$, $E_t$, $P_t$, and $\sigma_{max}$ which were evaluated to be larger for mode $N$. Such a correlation implies that the treatment-induced enhancement of different properties of materials is greatly determined by the energy density accumulated in the impact area during UIT.

By definition, integral parameters $E_t$ and $P_t$ should increase linearly with processing time $t$. However, in practical UIT, the dependence of physicochemical characteristics of materials on $t$ generally is not linear. In particular, both monotonic (but non-linear) and non-monotonic variation of microhardness, surface roughness, residual stress level,

**TABLE 1.** Evaluated impact treatment parameters of different alloys for two loading schemes (single-pin normal '$N$' and multi-pin sliding '$S$') and two pins' dimensions at $A_{uh} = 20$ µm. Pins' dimensions in mode $N$: $a$—dia = 17.5 mm, $l = 2.8$ mm, $m = 6.035$ g, $b$—dia = 19.0 mm, $l = 5.0$ mm, $m = 10.444$ g, pins' dimensions in mode $S$: $c$—dia = 4.9 mm, $l = 14.9$ mm, $m = 2.203$ g, $d$—dia = 5.2 mm, $l = 15.0$ mm, $m = 2.632$ g.

| Energy parameter | Impact power density $P_0$, kW/cm² ($\tau$, µs) | | | | Impact stress $\sigma_{max}$, MPa | | | |
|---|---|---|---|---|---|---|---|---|
| Pins-Mode/Sample | 1-$N$ | 3-$S$ | 5-$S$ | 7-$S$ | 1-$N$ | 3-$S$ | 5-$S$ | 7-$S$ |
| Zr31Ti18Nb[a, c] | 1.63[a] (2.13) | 1.22[c] (3.83) | 0.73[c] | 0.52[c] | 23.5 | 30.0 | 23.2 | 19.6 |
| AISI-321 steel,[c] | 1.90 (1.83) | 1.38 (3.39) | 0.83 | 0.59 | 47.7 | 61.0 | 47.3 | 39.9 |
| Ti6Al4V[a, c] | 1.79 (1.94) | 1.32 (3.55) | 0.79 | 0.57 | 27.3 | 34.8 | 27.0 | 22.8 |
| Zr31Ti18Nb[b, d] | 1.01[b] (3.42) | 1.04[d] (4.0) | 0.62[d] | 0.45[d] | 17.8 | 27.4 | 21.3 | 18.0 |

$\alpha$-martensite fraction, corrosion resistance and oxide layer thickness was observed in the range of impact treatment times up to 150, 240 and 360 s for different materials such as Zr$-$2.5% Nb [24], Ti6Al4V [14, 15], $\alpha$-Ti, AISI 321 steel [16, 18], AISI 304 steel [8], AISI D2 tool steel [21]. Therefore, when comparing the effectiveness of different treatment methods and effects of different treatment parameters, it appears reasonable to consider 'instantaneous' impact energy characteristics ($E_0$, $E_i$, $P_0$, $\sigma_{max}$) rather than integral ones ($E_t$, $P_t$), unless a linear variation of some materials characteristics in the studied processing time interval is obtained.

## 4. CONCLUSIONS

The maximum kinetic energy $E_p$ (or velocity $V_p$) and frequency $f_p$ of stochastic oscillations of pins being used in impact treatment of materials under two loading schemes (single-pin normal $N$ and multipin sliding/shearing $S$ impact loading modes) have been experimentally assessed for ultrasonic horn amplitudes ranging from 16 to 28 µm. By making use of the determined values of $E_p$, $V_p$ and $f_p$, a number of impact parameters, such as impact time $\tau$, maximum impact force $F$, maximum impact stress $\sigma_{max}$, impact energy density $E_0$ and impact power density $P_0$ injected in the contact area, impact energy intensity in the contact area $E_i$, total energy density $E_t$ and power density $P_t$ deposited during treatment time, were evaluated. It was found that $F$, $\sigma_{max}$, $E_0$, $E_i$, $E_t$, $P_0$ and $P_t$ increase with increasing horn amplitude and decrease with increasing number of pins used in mode $S$. The sample reciprocation in mode $S$ was demonstrated to result in a decrease in the density of deposited energy and its non-uniform distribution across the sample, with the $E_t$ and $P_t$ decreasing with increasing the amplitude of the sample reciprocating motion. The evaluated impact parameters characterizing the energetics of treatment process appear to be suitable for comparison of UIT-induced alterations under different conditions and understanding of impact-induced changes in physicochemical characteristics of various materials.

## REFERENCES

1.  J. Zhou, D. Retraint, Z. Sun, and P. Kanouté, *Surf. Coat. Technol.*, **349**: 556 (2018).
2.  C. Wang, C. Wang, L. Wang, Y. Lai, K. Li, and Y. Zhou, *Int. J. Adv. Manuf. Technol.*, **108**: 505 (2020).
3.  P. Peyre, X. Scherpereel, L. Berthe, C. Carboni, R. Fabbro, G. Béranger, and C. Lemaitre, *Mater. Sci. Eng. A*, **280**: 294 (2000).
4.  Z. D. Wang, G. F. Sun, Y. Lu, M. Z. Chen, K. D. Bi, and Z. H. Ni, *Surf. Coat. Technol.*, **385**: 125403 (2020).
5.  B. N. Mordyuk, Yu. V. Milman, M. O. Iefimov, G. I. Prokopenko, V. V. Silberschmidt,

M. I. Danylenko, and A. V. Kotko, *Surf. Coat. Technol.*, **202**: 4875 (2008).

6. A. Gill, A. Telang, S. R. Mannava, D. Qian, Y.-S. Pyoun, H. Soyama, and V. K. Vasudevan, *Mater. Sci. Eng. A*, **576**: 346 (2013).

7. E. Maleki, O. Unal, M. Guagliano, and S. Bagherifard, *Mater. Sci. Eng. A*, **810**: 141029 (2021).

8. D. A. Lesyk, H. Soyama, B. N. Mordyuk, V. V. Dzhemelinskyi, S. Martinez, N. I. Khripta, and A. Lamikiz, *J. Mater. Eng. Perform.*, **28**: 5307 (2019).

9. H. Soyama, *J. Mater. Process. Technol.*, **269**: 65 (2019).

10. R. Chen, H. Xue, and B. Li, *Metals*, **12**: 642 (2022).

11. H. L. Chan, H. H. Ruan, A. Y. Chen, and J. Lu, *Acta Mater.*, **58**: 5086 (2010).

12. S. Kanou, O. Takakuwa, S. R. Mannava, D. Qian, V. K. Vasudevan, and H. Soyama, *J. Mater. Process. Technol.*, **212**: 1998 (2012).

13. B. N. Mordyuk and G. I. Prokopenko, *Handbook of Mechanical Nanostructuring* (Ed. M. Aliofkhazraei) (Wiley-VCH Verlag GmbH & Co: 2015), p. 417.

14. M. A. Vasylyev, S. P. Chenakin, and L. F. Yatsenko, *Acta Mater.*, **103**: 761 (2016).

15. M. A. Vasylyev, S. P. Chenakin, and L. F. Yatsenko, *Acta Mater.*, **60**: 6223 (2012).

16. B. N. Mordyuk and G. I. Prokopenko, *J. Sound Vibration*, **308**: 855 (2007).

17. S. P. Chenakin, B. N. Mordyuk, and N. I. Khripta, *Vacuum*, **210**: 111889 (2023).

18. B. N. Mordyuk, G. I. Prokopenko, M. A. Vasylyev, and M. O. Iefimov, *Mater. Sci. Eng. A*, **458**: 253 (2007).

19. S. P. Chenakin, B. N. Mordyuk, and N. I. Khripta, *Appl. Surf. Sci.*, **470**: 44 (2019).

20. S. P. Chenakin, V. S. Filatova, I. N. Makeeva, and M. A. Vasylyev, *Appl. Surf. Sci.*, **408**: 11 (2017).

21. D. A. Lesyk, S. Martinez, V. V. Dzhemelinskyy, A. Lamikiz, B. N. Mordyuk, and G. I. Prokopenko, *Surf. Coat. Technol.*, **278**: 108 (2015).

22. V. K. Manzhosov, *Modeli Prodol'nogo Vozdeystviya* [Models of Longitudinal Impact] (Ul'yanovsk: UlGT: 2006) (in Russian).

23. C. Wang, R. Li, X. Bi, W. Yuan, J. Gu, J. Chen, M. Yan, and Z. Zhang, *J. Mater. Res. Technol.,* **22**: 853 (2023).

24. B. N. Mordyuk, O. P. Karasevskaya, and G. I. Prokopenko, *Mater. Sci. Eng. A*, **559**: 453 (2013).